Theor. Comput. Fluid Dyn. (2017) 31:579–593
DOI 10.1007/s00162-016-0419-4

ORIGINAL ARTICLE

Eurika Kaiser · Bernd R. Noack · Andreas Spohn · Louis N. Cattafesta · Marek Morzyński

Cluster-based control of a separating flow over a smoothly contoured ramp

Received: 14 February 2016 / Accepted: 21 December 2016 / Published online: 17 January 2017

Abstract The ability to manipulate and control fluid flows is of great importance in many scientific and engineering applications. The proposed closed-loop control framework addresses a key issue of model-based control: The actuation effect often results from slow dynamics of strongly nonlinear interactions which the flow reveals at timescales much longer than the prediction horizon of any model. Hence, we employ a probabilistic approach based on a cluster-based discretization of the Liouville equation for the evolution of the probability distribution. The proposed methodology frames high-dimensional, nonlinear dynamics into low-dimensional, probabilistic, linear dynamics which considerably simplifies the optimal control problem while preserving nonlinear actuation mechanisms. The data-driven approach builds upon a state space discretization using a clustering algorithm which groups kinematically similar flow states into a low number of clusters. The temporal evolution of the probability distribution on this set of clusters is then described by a control-dependent Markov model. This Markov model can be used as predictor for the ergodic probability distribution for a particular control law. This probability distribution approximates the long-term behavior of the original system on which basis the optimal control law is determined. We examine how the approach can be used to improve the open-loop actuation in a separating flow dominated by Kelvin–Helmholtz shedding. For this purpose, the feature space, in which the model is learned, and the admissible control inputs are tailored to strongly oscillatory flows.

Keywords Flow control · Markov model · Cluster analysis · Liouville equation · Flow separation · Feedback control

Communicated by Ati Sharma.

E. Kaiser (✉)
Mechanical Engineering Department, University of Washington, Seattle, WA 98195, USA
E-mail: eurika@uw.edu

E. Kaiser · B. R. Noack · A. Spohn
Institut PPRIME, UPR 3346 CNRS – Université de Poitiers – ENSMA, 86961 Futuroscope Chasseneuil, France

B. R. Noack
LIMSI-CNRS, UPR 3251, 91405 Orsay Cedex, France

B. R. Noack
Technische Universität Braunschweig, 38108 Braunschweig, Germany

L. N. Cattafesta
Florida Center for Advanced Aero-Propulsion, Florida State University, Tallahassee, FL 32310, USA

M. Morzyński
Chair of Virtual Engineering, Poznan University of Technology, 60-965 Poznań, Poland

1 Introduction

Controlling complex dynamical systems such as fluid flows is of great importance in science and engineering. Examples include drag reduction for greener transport systems, lift increase on airfoils, stabilization of combustion processes, reduction in pollutants from chemical processes and efficiency increase in energy harvesting systems such as wind turbines, to name a few. Closed-loop control which translates the continuously monitored system state into control actions is a particularly promising direction. We refer to [1] for a recent review on closed-loop control.

Of particular interest in control applications are certain statistical flow properties such as the average drag or lift which shall be mitigated or increased, respectively. However, their computation from trajectories may be misleading for several reasons. The time average is generally computed over a limited time span which makes it sensitive to transient behavior and biased as the trajectory may reside only in a confined state space region. Thus, very long integration times are required to ensure that the time average is sufficient. However, even without noise and external disturbances, small uncertainties in initial or boundary conditions may doom a deterministic system unpredictable. A well-studied example is the chaotic Lorenz system introduced by Lorenz [2], a simplified model for atmospheric convection with known sensitivity to initial conditions. Average properties over long time spans lead naturally to invariant probability measures on the attractor, i.e., these measures stay the same after transformation of the attractor. Ergodic measures, a subclass of invariant measures, are of particular interest as those time averages are equal to space averages following Birkhoff's ergodic theorem [3]. This assumption is often assumed when analyzing fluid flows: These flows are assumed to be ergodic, i.e., in the sense that they are statistically reproducible, allowing one to compute the statistical properties from ensemble averages. In this study, the system dynamics are modeled in terms of a Markov model, particularly a cluster-based reduced-order model (CROM) [4]. This simplification allows to compute many (statistical) properties exactly which are often good estimators for the analogous properties of the original system [5]. As a consequence of Birkhoff's ergodic theorem, controlling such statistical properties is strongly related to the control of the ergodic measure on the attractor.

The Markov model is a linear evolution equation for a probability distribution in the state space. Such evolution equations can be derived from the Navier–Stokes equation, starting with the linear Liouville equation of a suitable probability space. The Hopf [6] formalism for the Navier–Stokes equation is a prominent example. A simpler version constitutes the Liouville equation for a Galerkin system. The reader is referred to [7] for a detailed discussion. CROM is closely aligned with closure schemes, in which a stable fixed point represents the ergodic measure for the unsteady attractor in velocity space. While the control of a Liouville equation has not found much attention in fluid dynamics yet, it is studied widely in other fields such as atomic physics [8], biology [9] and robotics [10,11]. An extensive study on the optimal control of the Liouville equation is provided in [12]. The control of the Liouville equation can be interpreted as the manipulation of a particular system using a single controller over repeated realizations which correspond to different initial conditions. Thus, the control of the Liouville equation is a promising direction for systems that exhibit uncertainties in initial conditions and system parameters, e.g., due to disturbances.

In the present study, we extend the cluster-based reduced-order modeling approach for control applications building upon the presentation in Appendix B in [4]. The coarse-grained system dynamics are described by a transition probability matrix, which is based on a state space discretization. The incorporation of a control input results in a family of control-dependent transition matrices. The optimal control law which minimizes the asymptotic cost can be found by analysis of the transition matrices formulating a combinatorial optimization problem. We show how the control-oriented CROM can be learned from data and the optimal control law can be determined. The approach is illustrated for a separating flow over a smoothly contoured ramp characterized by Kelvin–Helmholtz shedding. Specifically, the present study aims to examine the improvement of an open-loop actuation known to result in a lock-in state which is associated with a time-averaged reduced but finite-size recirculation area. For that purpose, the model is learned in a subspace spanned by the first few POD modes associated with the forced flow under open-loop actuation. Finally, the best control law as predicted by the control-oriented CROM is compared to the best obtained from a brute-force search.

The present work is outlined as follows. In Sect. 2, the cluster-based control methodology is described including a general problem formulation and how the model can be inferred directly from data. The approach is applied to the benchmark problem of a separating flow over a backward-facing, smoothly contoured ramp. The main results are summarized in Sect. 3, and conclusions are provided in Sect. 4. In the appendix, a technique for visualizing the similarity of control laws is explained.

2 Cluster-based control methodology

2.1 Problem formulation

In this work, we are concerned with identifying a probabilistic low-order representation of the deterministic, fully nonlinear dynamics affected by control inputs and deriving optimal control laws with respect to an objective function. Generally, a dynamical system is represented as

$$\frac{\mathrm{d}}{\mathrm{d}t}\mathbf{a}(t) = \mathbf{F}(\mathbf{a}(t), \mathbf{b}(t)) \tag{1}$$

where the vector $\mathbf{a} \in \mathcal{A}$ denotes the system state in state space $\mathcal{A}$, vector $\mathbf{b}$ is the control input at time t, and $\mathbf{F}$ is the nonlinear propagator for the system state $\mathbf{a}$. We assume a full-state feedback ansatz for the control in the form

$$\mathbf{b} = K(\mathbf{a}) \tag{2}$$

where K represents the control law that maps states $\mathbf{a}$ to control actions $\mathbf{b}$. In optimal control, one seeks to determine an optimal control law K^{opt} which minimizes a cost function. The cost function, generally a function of the system state $\mathbf{a}$ and the control $\mathbf{b}$, defines the control objective through a performance measure and penalty function evaluating the cost of the applied control, and incorporates additional constraints. In flow control, the average drag or lift is often of interest. Let $h(\mathbf{a})$ be a function measuring a quantity of interest, e.g., the drag, along the trajectory $\mathbf{a}(t)$. For ergodic behavior, the temporal average $\langle h(\mathbf{a})\rangle_T := \lim_{T\to\infty} \int_0^T h(\mathbf{a}(t))\,\mathrm{d}t$ can be represented in terms of the spatial average $\langle h(\mathbf{a})\rangle_{\mathcal{A}} := \int_{\mathcal{A}} h(\mathbf{a})\, p(\mathbf{a})\,\mathrm{d}\mathbf{a}$ which is naturally defined by the probability density function (p.d.f.) $p(\mathbf{a})$. The average cost function can then be formulated as

$$J_K = \mathbb{E}^{\infty}\left[j(\mathbf{a}, \mathbf{b})|_{\mathbf{b}=K(\mathbf{a})}\right] = \int_{\mathcal{A}} j(\mathbf{a}, \mathbf{b})|_{\mathbf{b}=K(\mathbf{a})}\, p^{\infty}(\mathbf{a})\,\mathrm{d}\mathbf{a} \tag{3}$$

where $j(\mathbf{a}, \mathbf{b})$ is the local cost function, $\mathbb{E}^{\infty}$ is the expectation operator assuming transients have decayed and $p^{\infty}(\mathbf{a})$ is the asymptotic, i.e., long-run, p.d.f. A formulation of (3) for a finite time horizon is also possible, in which case p^{∞} would be replaced by the time-dependent $p(\mathbf{a}, t)$ and an additional integration over the time horizon would be considered leading to the average or cumulative costs over that time horizon. The control design task is to determine K^{opt} such that the p.d.f. $p^{\infty}(\mathbf{a})$ is as close as possible to a desired density for which the average cost J_K is minimized. The evolution of the p.d.f. is prescribed by a Liouville equation associated with the dynamical system (1),

$$\frac{\partial}{\partial t} p(\mathbf{a}, t) + \nabla_{\mathbf{a}} \cdot [p(\mathbf{a}, t)\, \mathbf{F}(\mathbf{a}, \mathbf{b})] = 0. \tag{4}$$

While the dynamical system (1) prescribes the evolution of a single trajectory in the state space, the Liouville equation (4) is a linear equation for the p.d.f. describing the distribution of a swarm of trajectories in the state space. Linked to the Liouville equation (4) is the Perron–Frobenius operator P_t [3], a linear evolution operator that maps the p.d.f. forward in time,

$$p(\mathbf{a}, t) = P_t\, p(\mathbf{a}(0)) \tag{5}$$

with $P_t := \exp(t\, L)$ where $L := -\nabla_{\mathbf{a}} \cdot \mathbf{F}(\mathbf{a}, \mathbf{b})$ is the Liouville operator. An invariant (or long-term) p.d.f. $p^{\infty}(\mathbf{a})$ constitutes a solution to the fixed-point equation $p(\mathbf{a}) = P_t\, p(\mathbf{a})$ for all $t \geq 0$. Note that a unique solution is not expected and there can be many or even infinitely many invariant p.d.f.s. For instance, if the dynamical system (1) possesses a stable fixed point $\mathbf{a}^{\star}$, the invariant density will be a peak supported over the fixed point, i.e., $p^{\infty}(\mathbf{a}) = \hat{\delta}(\mathbf{a}^{\star})$ where $\hat{\delta}$ is the Dirac delta function. If (1) exhibits a periodic limit cycle, the invariant density is the sum of delta functions supported over the points $\mathbf{a}_i^{\star}$, $i = 1, \ldots, N_{lc}$, constituting the limit cycle, i.e., $p^{\infty}(\mathbf{a}) = \sum_{i=1}^{N_{lc}} \hat{\delta}(\mathbf{a}_i^{\star})$. If (1) is a chaotic dynamical system, it consists of infinitely many unstable periodic orbits and therefore of infinitely many invariant densities. The reader is referred to [13] for more details on this topic.

2.2 Coarse-graining of state space

Let $\mathcal{A}_i, i = 1, \ldots, N_a$, be a discretization of the state space such that $\mathcal{A} = \cup_{i=1}^{N_a} \mathcal{A}_i$ with $\mathcal{A}_i \cap \mathcal{A}_j = \emptyset$ for $i \neq j$. Here, a data-driven partitioning method is pursued as outlined in Sect. 2.4.1 yielding a discrete number of clusters $\mathcal{A}_i$ with centroids $\mathbf{A}_i$ which serve as representative states for each cluster. Each state $\mathbf{a}(t)$ is connected to a symbol α representing the cluster $\mathcal{A}_\alpha$ to which $\mathbf{a}(t)$ belongs. Let the measurable equation, which maps the continuous state $\mathbf{a}$ to a discrete symbol α, be defined by

$$\alpha(t) = \chi(\mathbf{a}(t)) \in \{1, 2, \ldots, N_a\}. \tag{6}$$

The coarse-grained inverse mapping is defined by

$$\mathbf{a}^\circ(t) = \mathbf{A}_{\chi(\mathbf{a}(t))} \tag{7}$$

approximating the continuous state $\mathbf{a}$ by its closest cluster centroid, e.g., $\alpha = 1$ and $\mathbf{a}^\circ = \mathbf{A}_1$ if $\mathbf{a} \in \mathcal{A}_1$. The superscript $^\circ$ refers to the discrete-state approximation. The inverse operation is associated with a loss of information due to the coarse-graining process. Let the characteristic function be defined by

$$\chi_i(\mathbf{a}) = \begin{cases} 1 & \text{if } \mathbf{a} \in \mathcal{A}_i, \\ 0 & \text{if } \mathbf{a} \notin \mathcal{A}_i \end{cases} \quad \text{or} \quad \chi_i(\mathbf{a}) = \delta(\chi(\mathbf{a}) - i) \tag{8}$$

where δ is the Kronecker delta. The full-state feedback ansatz for the control is then

$$\mathbf{b}^\circ = K(\mathbf{a}^\circ) = K\left(\mathbf{A}_{\chi(\mathbf{a})}\right) = \kappa(\alpha) = \sum_{i=1}^{N_a} \mathbf{B}_i \, \chi_i(\mathbf{a}). \tag{9}$$

As a result of the discretization, the control $\mathbf{b}$ is piecewise constant where $\mathbf{B}_i$ are vectors of real numbers and denote the control applied in cluster $\mathcal{A}_i$. The control law κ, that maps discrete states $\mathbf{A}_i$ with symbols α into control actions $\mathbf{b}^\circ$, is considered stationary here, i.e., $\mathbf{B}_\alpha$ for a cluster α remains constant for all times. The optimal control law κ^{opt} minimizes the average cost function

$$J_\kappa = \mathbb{E}^\infty \left[j^\circ(\alpha, \mathbf{b})|_{\mathbf{b}=\kappa(\alpha)} \right] = \sum_{i=1}^{N_a} j^\circ(i, \kappa(i)) \; p_i^{\circ,\infty} \tag{10}$$

with the local cost function $j^\circ(\alpha, \mathbf{b})|_{\mathbf{b}=\kappa(\alpha)}$ evaluating the cost for the currently prevailing cluster α and the control input $\mathbf{B}_\alpha$ applied in this cluster. The vector $\mathbf{p}^{\circ,\infty}$ is the discrete asymptotic probability distribution for $t \to \infty$. This constitutes the solution to the fixed-point equation associated with the discrete-state Markov model

$$\frac{\mathrm{d}}{\mathrm{d}t}\mathbf{p}^\circ(t) = \mathsf{P}_\kappa^\circ \, \mathbf{p}^\circ(t). \tag{11}$$

This equation describes the temporal evolution of the probability vector $\mathbf{p}^\circ = [p_1^\circ, \ldots, p_i^\circ, \ldots, p_{N_a}^\circ]^T$ where p_i° is the probability that the trajectory $\mathbf{a}(t)$ resides in cluster $\mathcal{A}_i$. The matrix P_κ° prescribes the dynamics on the coarse-grained state space following a particular control law κ.

2.3 Discrete-time, discrete-state formulation

A further discretization level based on the time is considered. Let the floor function be defined as $\lfloor t \rfloor := \max\{l \in \mathbb{Z} \mid l \leq t\}$ [14]. A polymorphism for continuous-time and discrete-time variables is pursued for the purpose of a better readability. The measurement equation analogous to (6) is given by

$$\alpha^t = \chi(\mathbf{a}(\lfloor t \rfloor)) \in \{1, 2, \ldots, N_a\} \tag{12}$$

for discrete times t, where the superscript ^{t} is an index corresponding to multiple of Δt, and where χ is the characteristic function introduced above. The inverse discrete-time, coarse-grained mapping, connecting the instantaneous system state $\mathbf{a}$ to its closest centroid $\mathbf{A}_\alpha$ for $\mathbf{a} \in \mathcal{A}_\alpha$, is given by

$$\mathbf{a}^{\bullet,t} = \mathbf{A}_{\chi(\mathbf{a}(\lfloor t \rfloor))}. \tag{13}$$

The superscript $^\bullet$ refers here to the discrete-state, discrete-time representation of quantities. The full-state feedback ansatz for the control becomes

$$\mathbf{b}^\bullet = K(\mathbf{a}^\bullet) = K\left(\mathbf{A}_{\chi(\mathbf{a}(\lfloor t \rfloor))}\right) = \kappa(\alpha) \tag{14}$$

realizing the time delay. The optimal control law κ^{opt} shall minimize the average cost function

$$J_\kappa = \mathbb{E}^\infty\left[j^\bullet(\alpha, \mathbf{b})|_{\mathbf{b}=\kappa(\alpha)}\right] = \sum_{i=1}^{N_a} j^\bullet(i, \kappa(i))\, p_i^{\bullet,\infty} \tag{15}$$

with local cost function $j^\bullet(\alpha, \mathbf{b})|_{\mathbf{b}=\kappa(\alpha)}$. The asymptotic probability vector $\mathbf{p}^{\bullet,\infty}$ is a solution to the fixed-point equation of the discrete-state, discrete-time Markov model, giving rise to a Markov chain, which describes consecutive distributions by the recursive formula

$$\mathbf{p}^{\bullet,t+1} = \mathsf{P}_\kappa^\bullet\, \mathbf{p}^{\bullet,t}, \quad t = 0, 1, 2, \ldots \tag{16}$$

with the cluster transition probability matrix $\mathsf{P}_\kappa^\bullet$ prescribing the dynamics following a particular control law κ.

The Markov model (16) can be derived from (4) using Ulam's method [15,16] which is classically used in dynamical systems to determine a finite rank approximation of the Perron–Frobenius operator (5). Ulam's method involves a Galerkin projection of the Liouville equation (4) onto a particular set of basis functions. Recently, [4] showed that the cluster-based reduced-order modeling approach can be interpreted as a generalization of Ulam's method for which the discretization is obtained through a data-driven clustering algorithm. A discussion on the Markov property is provided in Sect. 2.2.3 of [4].

2.4 Identification of the control-oriented CROM from data

In this section, we briefly outline the state space discretization process using the aforementioned clustering algorithm and how the model in (16) can be inferred from data.

2.4.1 Discrete domain decomposition using cluster analysis

Cluster analysis is a part of machine learning and pattern recognition [17] which learns automatically from data. The aim of cluster analysis is to find a hidden grouping among a given set of observations, here in particular the ensemble $\{\mathbf{a}^m\}_{m=1}^M$. A prominent clustering algorithm is k-means clustering [18], which groups kinematically similar flow states into a low number N_a of clusters $\mathcal{A}_i$, $i = 1, \ldots, N_a$, such that the similarity of observations in the same cluster is maximized while the similarity of observations belonging to different clusters is minimized. Here, the *dissimilarity* between observations $\mathbf{a}^m$ and $\mathbf{a}^n$ is measured using the Euclidean distance

$$D(\mathbf{a}^m, \mathbf{a}^n) := ||\mathbf{a}^m - \mathbf{a}^n||_2. \tag{17}$$

The cluster centroid $\mathbf{A}_i$ of $\mathcal{A}_i$ is defined as the average of observations belonging to the cluster $\mathbf{A}_i := \frac{1}{n_i} \sum_{\mathbf{a}^m \in \mathcal{A}_i} \mathbf{a}^m$ where n_i is the total number of observations in cluster $\mathcal{A}_i$. The quality of the algorithm is monitored by the total cluster variance, $J_{\text{ca}}\left(\mathbf{A}_1, \ldots, \mathbf{A}_{N_a}\right) = \sum_{i=1}^{N_a} \sum_{\mathbf{a}^m \in \mathcal{A}_i} ||\mathbf{A}_i - \mathbf{a}^m||_2^2$. The algorithm starts with an initial set of centroids and then iteratively improves them by minimizing the total cluster variance. The set of optimal centroids is thus the solution of the optimization problem

$$\mathbf{A}_1^{\text{opt}}, \ldots, \mathbf{A}_{N_a}^{\text{opt}} = \arg \min_{\mathbf{A}_1, \ldots, \mathbf{A}_{N_a}} J\left(\mathbf{A}_1, \ldots, \mathbf{A}_{N_a}\right). \tag{18}$$

The reader is referred to [4] for more details.

2.4.2 Control-oriented cluster-based reduced-order model

The propagator of the Markov model (16) for the coarse-grained dynamics is directly inferred from data. A multidimensional array $\mathsf{Q} \in \mathbb{R}^{N_a \times N_a \times N_b}$ of control-dependent transition probabilities, where N_b denotes the number of admissible control inputs, is constructed with elements

$$\mathsf{Q}_{ijb} := \frac{\text{card}\{\mathbf{a}^m | \mathbf{a}^m \in \mathcal{A}_j \text{ and } \mathbf{a}^{m+1} \in \mathcal{A}_i \text{ and } b^m\}}{\text{card}\{\mathbf{a}^m \in \mathcal{A}_j\}} = \text{Prob}\left(\alpha^{t+1} | \alpha^t, b^t\right) \tag{19}$$

where card denotes cardinality. The element Q_{ijb} constitutes the conditional probability that at time $t+1$ the trajectory is in cluster $\mathcal{A}_i$ under the condition that at the previous time step t the trajectory was in cluster $\mathcal{A}_j$ and control b was applied. Array Q is directly inferred from data based on the relative frequencies of cluster transitions. The control-oriented cluster transition matrix (CTM) P_κ for a particular control law κ is constructed from the data array Q_{ijb} as

$$\mathsf{P}_\kappa := \left[\mathbf{q}_{1\,\kappa(1)} \ \cdots \ \mathbf{q}_{j\,\kappa(j)} \ \cdots \ \mathbf{q}_{N_a\,\kappa(N_a)}\right]. \tag{20}$$

with $\mathbf{q}_{j\kappa(j)} = [\mathsf{Q}_{1\,j\kappa(j)}, \ldots, \mathsf{Q}_{N_a\,j\kappa(j)}]^T$ by selecting the columns $\mathbf{q}_{j\kappa(j)}$ specified by the control law κ. The temporal evolution of a general cluster probability vector $\mathbf{p} = [p_1, \ldots, p_{N_a}]^T$ can be studied by powers of the CTM. Having an initial probability distribution $\mathbf{p}^0$, the cluster probability vector at time t is

$$\mathbf{p}^t = \mathsf{P}_\kappa^t \, \mathbf{p}^0. \tag{21}$$

The cluster probability vector has non-negative probabilities, i.e., $p_i^t \geq 0$, and fulfills the normalization condition $\sum_{i=1}^{N_a} p_i^t = 1$ for each time step t. The asymptotic probability distribution is obtained by

$$\mathbf{p}^\infty := \lim_{t \to \infty} \mathsf{P}_\kappa^t \, \mathbf{p}^0. \tag{22}$$

If $\mathbf{p}^t$ converges to a unique, stationary probability vector, the system can said to be *ergodic*, in the sense that it will be probabilistically reproducible: Regardless of the initial region of state space in which it is sampled, the ensemble mean will converge in the infinite time limit to the time mean. Each propagator P_κ defines a time-homogeneous Markov chain with well-known properties [19]: (1) The propagator P_κ is a stochastic matrix with non-negative elements, i.e., $\mathsf{P}_{ij} \geq 0 \ \forall \ i, j$, and the elements of each column sum up to unity, i.e., $\sum_{i=1}^{N_a} \mathsf{P}_{ij} = 1 \ \forall \ j$. These properties preserve the normalization condition of the probability vector. (2) The sequence of probability vectors $\mathbf{p}^t$, $t = 0, 1, 2, \ldots$, has no long-term memory, i.e., the state at iteration $t+1$ only depends on the tth state and not on any previous iteration. (3) The absolute values of all eigenvalues of this matrix do not exceed unity, which excludes a diverging vector sequence. (4) There exists an eigenvalue $\lambda_1(\mathsf{P}_\kappa) = 1$ with algebraic multiplicity 1 and all other eigenvalues satisfy $|\lambda_i(\mathsf{P}_\kappa)| < 1$ for $i = 2, \ldots, N_a$. This is a consequence of the Perron–Frobenius theory for non-negative matrices [19]. The eigenvector $\mathbf{p}^{*1}$ associated with the dominant eigenvalue $\lambda_1(\mathsf{P}_\kappa)$ fulfills the fixed-point equation $\mathsf{P}_\kappa \, \mathbf{p}^{*1} = \mathbf{p}^{*1}$. Since $|\lambda_i(\mathsf{P}_\kappa)| < 1$ for $i = 2, \ldots, N_a$, the vector $\mathbf{p}^{*1}$ is the only one that survives infinite iterations. Mathematically, the stationary probability vector $\mathbf{p}^\kappa$ must be identical with the eigenvector $\mathbf{p}^{*1}$ associated with the dominant eigenvalue $\lambda_1 = 1$ and thus is a fixed point to (21) for any t . If, however, $\mathbf{p}^\infty$ is oscillatory or non-stationary, the system will not be probabilistically reproducible, displaying a more complicated connection between the initial sampling region and its convergence properties.

2.5 Control design using CROM

In the following, the discrete-state, discrete-time formulation of Sect. 2.3 is considered and the superscript "•" is dropped. A general ansatz for the control law for multi-input control is given by

$$\kappa(\alpha) = \sum_{i=1}^{N_a} \mathbf{B}_i \, \chi_i(\mathbf{a}) \tag{23}$$

where the $\mathbf{B}_i$'s are real-valued vectors, a specific control input for each cluster i with length corresponding to the number of inputs. Note that $\chi_i(\mathbf{a})$ is the characteristic function defined in (8) which assumes values 0 or 1

depending on whether the current state $\mathbf{a}$ lies in cluster $\mathcal{A}_i$. The specific cluster-dependent control action can be selected from a predefined set of admissible control inputs.

Since the number of clusters and the number of admissible control actions are assumed to be fixed, there exist a fixed number of possible control laws. For instance, let us assume that the state space is discretized into $N_a = 10$ clusters, and we consider single-input control and the scalars B_i can assume two possible values, namely 0 or 1 representing an on–off controller (also referred to as bang–bang controller). Then, the possible control laws are defined by all combinations of 0's and 1's. Let further the control law be represented by a string of 0's and 1's of length N_a. The number of 1's in this string shall be denoted as N_v. The total number of combinations of how N_v 1's can be arranged in this string, i.e., on N_a clusters, is given by $\sum_{0\leq N_v\leq N_a} C(N_a, N_v) = \sum_{0\leq N_v\leq N_a} \binom{N_a}{N_v} = 2^{N_a}$. For the given example of $N_a = 10$ clusters, the total number of control laws is thus $\sum_{0\leq N_v\leq 10} \binom{10}{N_v} = 2^{10} = 1024$:

$$\kappa^0(\alpha) = B_{0000000000} = 0, \tag{24a}$$

$$\kappa^1(\alpha) = B_{0000000001} = B_1\,\delta(\alpha - 1), \tag{24b}$$

$$\vdots$$

$$\kappa^{386}(\alpha) = B_{0110000010} = B_2\,\delta(\alpha - 2) + B_8\,\delta(\alpha - 8) + B_9\,\delta(\alpha - 9), \tag{24c}$$

$$\vdots$$

$$\kappa^{1023}(\alpha) = B_{1111111111} = \sum_{i=1}^{N_a} B_i\,\delta(\alpha - i)\,, \tag{24d}$$

where $B_{\mathsf{xxxxxxxxxx}}$ with $\mathsf{x} \in \{0, 1\}$ refers to the string representing the control law. Terms in the series which are always zero independent of the state are neglected.

The control design task consists of determining the control law that minimizes the average cost function (15). For any control law $\kappa(\alpha)$ (or $\kappa^l(\alpha)$, respectively) such a cost J_κ can be simply evaluated,

$$J_\kappa = \sum_{i=1}^{N_a} j(i, \kappa(i))\, p^{\infty}_{\kappa,i} = \sum_{i=1}^{N_a} j(i, \kappa(i))\, p^{*1}_{\kappa,i}, \tag{25}$$

exploiting that the dynamics introduced by a control law $\kappa(\alpha)$ are described by P_κ. This is a critical enabler for the control design as it allows the prediction of the invariant probability distribution $\mathbf{p}^{\infty}_{\kappa}$ by the eigenvector $\mathbf{p}^{*1}_{\kappa}$ associated with the dominant eigenvalue λ^1_κ of P_κ (see Sect. 2.4.2). The local cost function $j(\alpha, \kappa(\alpha)) = j_\alpha(\alpha) + \gamma\, j_b(\kappa(\alpha))$ encodes the costs j_α associated with the prevailing cluster α, e.g., the mean lift or drag in that cluster, and j_b associated with the control action $\kappa(\alpha)$ applied when the trajectory resides in that cluster. The probabilities $\mathbf{p}^{\infty}_{\kappa}$ or $\mathbf{p}^{*1}_{\kappa}$, respectively, represent the average residence or sojourn times of the trajectory in each of the clusters. Thus, each cluster-specific cost is weighted by the time duration the cluster is visited.

Having determined J_κ for all κ, the optimal control law is then given by

$$\kappa^{\mathrm{opt}}(\alpha) = \underset{b=\kappa(\alpha)}{\arg\min}\, J_\kappa. \tag{26}$$

The control law from (26) is referred to as greedy law or policy as it greedily selects the best control actions based on J. The greedy law has to be taken with care as it could perform potentially suboptimal in the long run, in some cases leading to the worst-case scenario [20,21]. More generally, a possible solution is to use a learning algorithm which includes switches between exploration and exploitation phases such that the control law does not select suboptimal actions [22].

3 Control of a separating flow over a smooth ramp

3.1 Flow configuration and numerical simulation

The two-dimensional flow is described by a Cartesian coordinate system in which the location vector is denoted by $\mathbf{x} = (x, y)^T$ where x is in flow direction and y is the direction perpendicular to x. The two-dimensional velocity vector is denoted by $\mathbf{u}(\mathbf{x}, t) := (u, v)^T$ where u and v are the velocities in x- and

y-direction, respectively, and t denotes the time. The pressure is represented by P. The non-dimensionalized Navier–Stokes and continuity equations are

$$\begin{aligned} \partial_t \mathbf{u} + \nabla \cdot (\mathbf{u}\,\mathbf{u}) &= -\nabla P + \frac{1}{Re}\Delta \mathbf{u} + \mathbf{G}\, b, \\ \nabla \cdot \mathbf{u} &= 0 \end{aligned} \tag{27}$$

where $Re = U_\infty L/\nu = 7700$ is the Reynolds number based on the length L of the flat plate located upstream of the contoured ramp at $x \in [0, 1]$ [23]. Actuation is implemented via a steady local force field in y-direction denoted by $\mathbf{G}$. The function b is the time-dependent control input amplitude and has compact support in a circular region. It is centered at $x = 1$ and the y-position is chosen such that the circular region is mostly inside the boundary layer. The computational domain Ω for the flow comprises

$$\Omega := \{(x, y) : -1 \le x \le 10,\ f(x) \le y \le 2.6\}\,. \tag{28}$$

The domain is discretized as mixed Taylor–Hood elements [24] on an unstructured triangular mesh comprising 8567 nodes with increased resolution around the leading edge, in the boundary layer and in the shear layer region. A quadratic finite element method formulation is used to discretize the evolution equations with no-slip boundary on the ramp and stress-free outflow. A detailed description of the solver can be found in [25,26]. A rectangular velocity profile $\mathbf{U}\infty := \mathbf{u}(x = 1, y) = (1, 0)^T$ is used as inflow. The numerical time step is 0.005 and the sampling period of the snapshots is 20, i.e., $\Delta t = 0.1$. The topography of the smooth ramp is described by a polynomial shape of order 7 [23,27]. Due to an adverse pressure gradient induced by the gradual change in curvature along the ramp contour, the flow separates from the wall leading to a large recirculation area and the development of a convectively unstable free shear layer. The latter gives rise to the Kelvin–Helmholtz instability by which two-dimensional perturbations are spatially amplified that eventually roll up into vortices [28]. This recirculation area is characterized by fluid moving in the opposite direction of the flow. Increased pressure drag and reduced lift forces are often associated with the extent of similar recirculation areas on airfoils. In this study, the objective is to reduce the recirculation area in order to attenuate the pressure drag. The mean recirculation area $\langle R(t)\rangle$ is defined by

$$\langle R(t)\rangle = \frac{1}{T_2 - T_1} \int_{T_1}^{T_2} \int_{\Omega_R} H(-u(\mathbf{x}))(t)\, \mathrm{d}\mathbf{x}\, \mathrm{d}t \tag{29}$$

where H denotes the Heaviside function, Ω_R is the chosen region for evaluation, and the limits for the temporal integration are chosen such that the transient is excluded, i.e., $T_1 = 25 \approx 4.4\, T_{\mathrm{sh}}$ and $T_2 - T_1 = 70 \approx 7.92\, T_{\mathrm{sh}}$ with the shedding period $T_{\mathrm{sh}} = 1/f_{\mathrm{sh}}$ of the uncontrolled flow. The estimation of the recirculation area is an approximation assuming that the recirculation area corresponds to those regions where the streamwise velocity component is negative. The average cost function to assess the performance of the control is defined by

$$J = \frac{\langle R(t)\rangle}{\langle R_0(t)\rangle} \tag{30}$$

normalized by the mean recirculation area $\langle R_0(t)\rangle$ of the uncontrolled flow. An instantaneous and mean plot of the recirculation area of the uncontrolled flow are shown in Fig. 1.

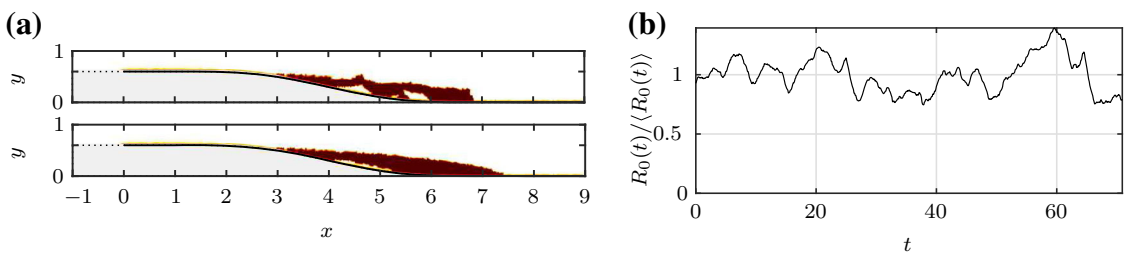

Fig. 1 Recirculation area (shown in *red*) of **a**, *top*, an instantaneous velocity snapshot and (**a**, *bottom*) the mean flow, and **b** time series of the normalized recirculation area for the uncontrolled flow (color figure online)

3.2 Control results

In this section, we develop an on–off controller which exploits the effectiveness of periodic open-loop actuation. We consider single-output control laws of the specific form

$$\kappa(\alpha) = \sum_{i=1}^{N_a} B_i\, \chi_i(\mathbf{a}) = \sum_{i=1}^{N_a} \hat{B}_i\, \sin(\omega_p\, t)\, \chi_i(\mathbf{a}) \tag{31}$$

where $\hat{B}_i$ denotes a fixed amplitude for the actuation which can assume values $\{0, 2\}$. Thus, the cluster-dependent control actions B_i become time-dependent scalars and the control law is uniquely determined by the amplitude $\hat{B}_i$, which determines whether the periodic excitation is turned off ($\hat{B}_i = 0$) or on ($\hat{B}_i = 2$), respectively, depending on the prevailing cluster $\mathcal{A}_i$. A suitable angular frequency for ω_p can be easily determined using open-loop periodic forcing and selecting the frequency for which the recirculation area has decreased most. For the considered flow simulation, this frequency has been determined as $f_p = 0.45$. Thus, the control law is based on the best periodic excitation exploiting that this frequency is known to be effective. The system state $\mathbf{a} := [a_1, \ldots, a_N]^T$ is given by

$$\mathbf{a}(t_m) = \int_{\Omega} \mathbf{\Phi}_N^T\, \mathbf{u}^m(\mathbf{x})\, \mathrm{d}\mathbf{x} \tag{32}$$

projecting the instantaneous velocity snapshot $\mathbf{u}^m$ onto the first $N_{\mathrm{pod}} = 10$ proper orthogonal decomposition [29] (POD) modes $\mathbf{u}_i^p(\mathbf{x})$ constituting the columns of $\mathbf{\Phi}_N := [\boldsymbol{\phi}_1^p, \ldots, \boldsymbol{\phi}_N^p]$. These POD modes are computed from a snapshot ensemble sampled of a flow under periodic excitation with $f_p = 0.45$.

The data for the cluster and model identification is collected by applying the actuation signal (see Fig. 2), which comprises time spans where the control is either turned on or off. The temporal signal of the POD coefficient vector $\mathbf{a}$ is computed from the acquired snapshot set according to (32). The state space is discretized by applying an unsupervised clustering algorithm (see Sect. 2.4.1) to the data ensemble $\{\mathbf{a}^m\}_{m=1}^M$ with the number of clusters $N_a = 10$. The cluster centroids based on the vorticity of the snapshots belonging to each cluster are displayed in Fig. 3. Most centroids, $i = 2, 3, 4, 5, 6, 7, 8$, represent the lock-in state when periodically exciting the flow. The remaining centroids, $i = 1, 9, 10$, are associated with the uncontrolled flow. Transient states are not resolved into individual clusters.

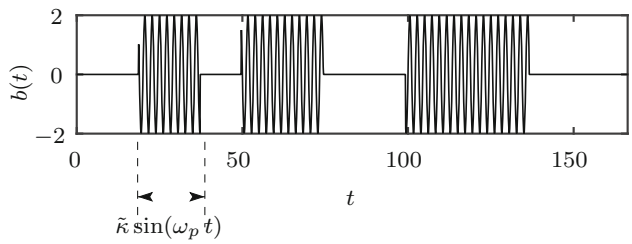

Fig. 2 Actuation signal for model identification switching between phases where $b = \tilde{\kappa}\, \sin(\omega_p\, t)$ and $b = 0$

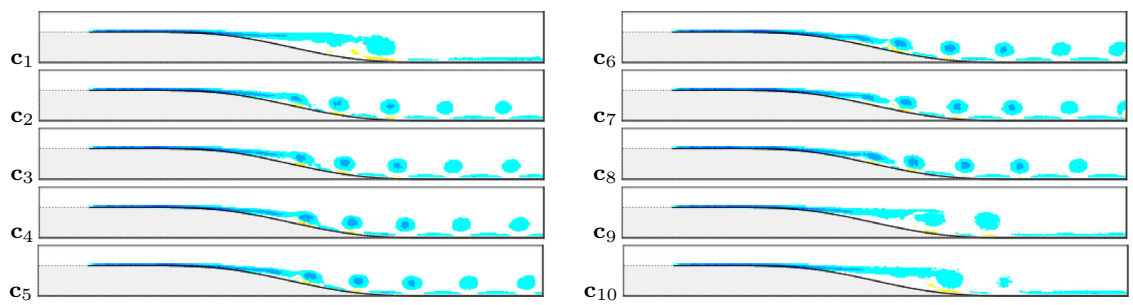

Fig. 3 Cluster vorticity centroids $\mathbf{c}_i(\mathbf{x}) = \nabla \times (1/n_i \sum_{\mathbf{a}^m \in \mathcal{A}_i} \mathbf{u}^m(\mathbf{x}))$ for each cluster $\mathcal{A}_i$

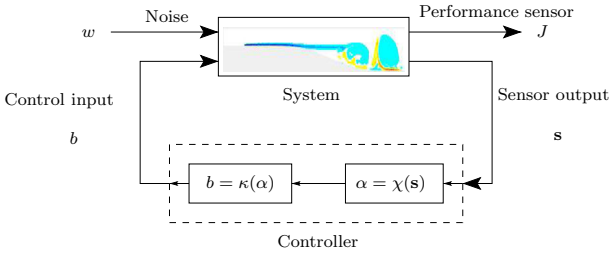

Fig. 4 Schematic of feedback control loop

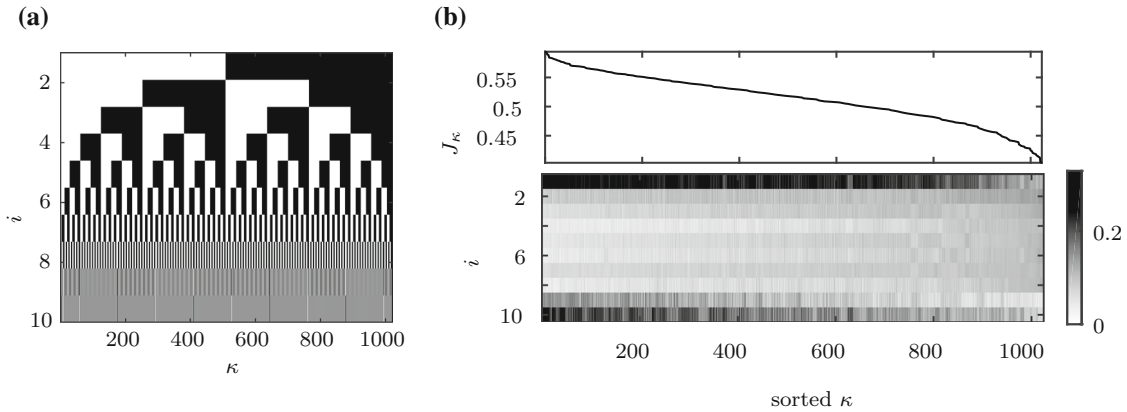

Fig. 5 Optimal control law: **a** set of control laws κ^l, $l \in \{1, \ldots, 1024\}$, **b**, *top* their average cost J_κ [see (25)], and **b**, *bottom* the eigenvector $\mathbf{p}^{*1}$ corresponding to the dominant eigenvalue λ_1 of the associated transition matrix P_κ. The symbols *open square* and *filled square* depict the control state "off," i.e., $\chi_\alpha(\mathbf{a}) = 0$, and "on," i.e., $\chi_\alpha(\mathbf{a}) = 1$, respectively. Note that the control laws in both figures in (**b**) are sorted according to descending costs J_κ. Thus, the best control law corresponds to the right most control law

A local cost function $j(i)$ is associated with each cluster $\mathcal{A}_i$

$$j(i) = \frac{1}{n_i} \sum_{\mathbf{a}^m \in \mathcal{A}_i} R(t_m). \tag{33}$$

in terms of the recirculation area averaged over the snapshots belonging to cluster $\mathcal{A}_i$. The desirability of a particular cluster is thus represented by this cost taking into account the control objective (compare Sect. 3.1), while the control input is not penalized here. The control-dependent transition probabilities are computed according to (19) in Sect. 2.4.2 and are used to construct the cluster transition matrices P_κ prescribing the dynamics under control law κ.

The feedback control loop is displayed in Fig. 4. A sensor reading $\mathbf{s}$ is fed back to the controller in which first the prevailing cluster α is computed and then the control input b is determined based on the control law $\kappa(\alpha)$. Here, full-state information is assumed, i.e., $\mathbf{s} = \mathbf{a}$. A realistic system is generally affected by noise which is neglected in this study. A sensor measures the performance J of the control law with regard to the control objective. The set of control laws to be evaluated is shown in Fig. 5a. The abscissa depicts the control laws $\kappa^l(\alpha)$ and the ordinate corresponds to the cluster index i, which is selected by the prevailing cluster α. The asymptotic probability vectors $\mathbf{p}_\kappa^\infty \, \forall \kappa$ originating from the dynamics prescribed by P_κ can be predicted by the corresponding eigenvector $\mathbf{p}_\kappa^{*,1}$ (see Fig. 5b, bottom). The associated average cost (25) is displayed in Fig. 5b, top. The optimal control law $\kappa^{\text{opt}} = B_{0010101111}$ as determined by (26) is the right most. The left most probability vectors are clearly in favor of cluster 1, 9 and 10, and have comparably low probabilities in the remaining clusters. For these control laws, the flow remains mostly in the clusters corresponding to the uncontrolled flow (compare Fig. 3). In contrast, for those probability vectors on the right-hand side, the condition is reversed: the probabilities of clusters 1, 9 and 10 are much lower and those of the remaining clusters have increased. Thus, these control laws direct the flow to clusters associated with smaller recirculation area.

This analysis is based on the prediction of the models P_κ. In addition, all control laws are evaluated in the numerical simulation. The mean input energy is defined by $J_b = \langle b^2(t) \rangle = \frac{1}{T_2 - T_1} \int_{T_1}^{T_2} b^2(t) \, \mathrm{d}t$ based on the

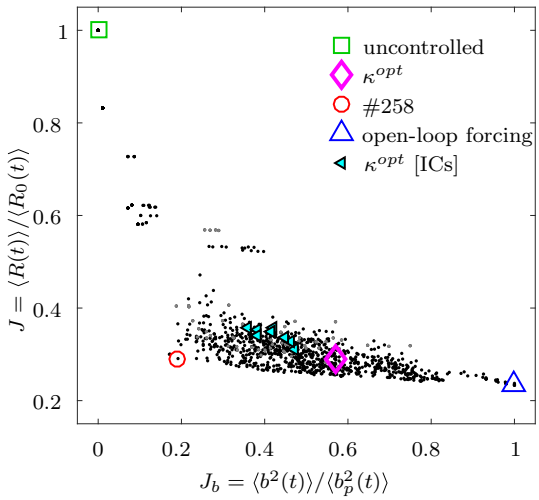

Fig. 6 Pareto diagram of control laws showing the trade-off between reduction in the recirculation area and the required control effort

applied actuation signal b to assess the required control effort. A Pareto diagram of the control results is shown in Fig. 6. The axes of Fig. 6 are normalized based on the mean recirculation area of the uncontrolled flow and the mean input energy of the open-loop periodic forcing. The periodically forced flow has clearly the smallest recirculation area (23%). The optimal control law κ^{opt} produces a slightly larger recirculation area (28%). Note that the asymptotic average cost (with respect to the local cost) of κ^{opt} predicted by the model is about 0.4, while its evaluation yields approximately 0.46. Interestingly, the optimal control law yields a comparable J while considerably decreasing the required input energy by 43%. There is a trade-off: the recirculation area cannot be reduced without increasing the required input energy. If these effects are weighted evenly, the best trade-off is achieved by control law #258 ($B_{0100000010}$) with a recirculation area corresponding to 29% and a reduction in the input energy by 81%. This control law can be attributed to the synchronization of the flow to recurring peaks in the actuation with frequency f_p. The performance of control law κ^{opt} is also compared for different initial conditions (shown as ◀ symbols in Fig. 6), which are chosen as the closest snapshot to each of the centroids. The dependency of κ^{opt} on the initial state may be reduced by increasing the number of clusters to improve the resolution of transient processes and by considering longer and richer training data for the model, that sufficiently captures these transients, but may also originate from a sensitivity of the flow to initial conditions.

The analysis of the similarity of the actuation time series resulting from applying the control laws can give additional insights into the cluster-based approach. In Fig. 7a, a two-dimensional plot is displayed where each circle corresponds to a particular control law κ^l. The distance between these circles depicts their respective similarity as defined in (34) in the appendix. The color of the circles depicts the percentile rank of J associated with a particular control law, e.g., 90 and higher correspond to the best 10% of control laws. The percentile rank is computed using the nearest rank method. The control laws are arranged in several groups $G_k, k = 1, \ldots, 8$, (numbered in circles for later reference): two lower bright groups corresponding to poorly performing control laws, three large groups with mixed performance on the left-hand side and three groups of similar size on the right-hand side with predominantly better performance. The grouping of the clusters is influenced by the state space discretization. For example, the uncontrolled flow exhibits mainly clusters 1, 9, 10 with negligible probability for clusters 2 and 3. Any control law of the form $B_{000\text{x}\text{x}\text{x}\text{x}\text{x}00}$, where x can be any control value, must be similar to $b(t) = 0\,\forall t$ and perform like the uncontrolled flow and thus belong to the same group in Fig. 7a. This interpretation is corroborated by the results in Fig. 7b, c. Figure 7b shows the probability, that actuation is *on*, i.e., $\hat{B}_i \neq 0$, in the particular cluster, per group and cluster. Figure 7c gives additional complementary information with respect to the performance. Several observations can be made: (1) The non- or poorly performing control laws in G_6 and G_7 have all no actuation in at least clusters 1, 9 and 10. (2) *All* control laws κ^l with $l \in \{G_1, G_4, G_5, G_7\}$ (upper right-hand side of Fig. 7a) have actuation $\hat{B}_2 \neq 0$ in cluster 2 in contrast to those remaining ones on the left-hand side, which *all* have actuation off. In particular, the best performing 25% control laws have all $\hat{B}_2 \neq 0$. (3) The distribution in the γ_2-direction can be explained by the actuation in clusters 1,9 and 10. If more of these clusters have actuation $\hat{B}_i \neq 0, i \in \{1, 9, 10\}$, the control law

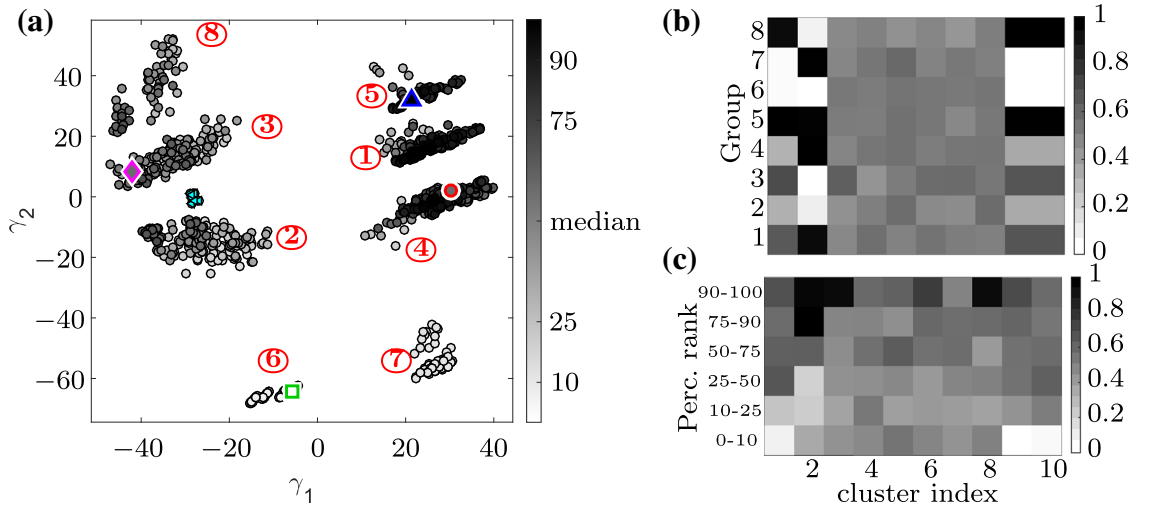

Fig. 7 Control law analysis: **a** two-dimensional visualization of the control laws based on their similarity and colored by the percentile rank of their performance J, and **b** percentage of control laws in each group [according to numbering in *red circles* in (**a**)] that have the control law *on* in a cluster, and **c** similar analysis such as (**b**) but with respect to the performance of the control laws. For details see text (color figure online)

is located farther away from the poorly performing control laws in G_6 and G_7. (4) Actuation in clusters 2, 3, and 8, i.e., actuation only at particular phases of the flow, is crucial to obtain a good performance.

As a final remark, we assess the complexity of the approach by comparing the number of snapshots of the training data for the CROM-based control law and that collected from the brute-force search. For the cluster and model identification steps $M = 1650$ snapshots have been analyzed comprising few transients between the controlled and unforced flow which is comparable to other model-based approaches. In contrast, $M_{\text{tot}} = N_v^{N_c} \cdot M = 2^{10} \cdot 700 = 716800$ snapshots have been collected in the exhaustive search. Thus, the required training data amounts to 0.23% compared to brute-force search.

4 Conclusions and perspectives on future directions

The present study proposes a cluster-based control strategy for the determination of optimal control laws for unsteady fluid flows. This framework builds upon a cluster-based reduced-order model (CROM) which translates high-dimensional, nonlinear dynamics into low-dimensional, probabilistic dynamics. The control problem is formulated as a combinatorial optimization problem for the average cost. The ability to find the optimal control law in an unsupervised manner highlights the generic applicability of the framework to other dynamical systems.

The approach is demonstrated for a separating flow over a smooth ramp with the aim to reduce the mean recirculation area. In particular, the control-oriented CROM is learned in the subspace spanned by the dominant POD modes associated with the flow state under the best open-loop periodic forcing to examine whether improvements can be achieved. An important observation is the trade-off between the recirculation area and the required control effort. One cannot be decreased without increasing the other. Intriguingly, while the number of clusters is too low to resolve the transition process, considerably reductions in the input energy can be achieved through the optimal control law while yielding a similarly reduced recirculation area with respect to periodic excitation. One particularly efficient control law is attributed to the synchronization of the flow to recurring peaks in the actuation. Similarly to sinusoidal forcing, the flow exhibits a lock-in state with the actuation frequency. As a consequence, the flow separates later with much smaller vortices shedding closely along the wall.

Low-dimensional modeling and control based on a coarse state space discretization have gained more attention in the fluids community over the last decade as it enables the simplification of computational algorithms. In particular, the k-means algorithm has emerged as an efficient data-driven method to group kinematically similar states leading, e.g., to a hybrid feature extraction approach combining centroidal Voronoï tessellation with proper orthogonal decomposition [30]. Recent developments in transition matrix models show that these

can be an appealing alternative to deterministic models due to their simplicity and predictive capabilities. [31] developed a transition matrix model describing the switching behavior between different coherent structures in pipe flow. More recently, in [32] an optimized transition matrix model has been inferred from data to predict the evolution of an observable related to the El Nino phenomena. We briefly mentioned CROM's connection to the Perron–Frobenius operator. Approximations of this operator can be used to determine so-called almost-invariant sets, coherent state space regions in which the trajectory resides for a long time before switching to another set. In [33], regions of these almost-invariant sets [34, e.g.] have been related to linear and nonlinear dynamical behavior, respectively, of the system. While the use of transition matrix models for analysis and as a predictive tool has been very successful, their exploitation for the control of fluid flows is still a challenging endeavor. One direction is model predictive control based on the Markov model. Markov models are appealing as statistical properties can be computed exactly for the models and these are often good approximations for the real system. When applying control, the system dynamics change and a previously learned model may become invalid and looses its predictive power. A model predictive control variant where the model is continuously updated and used as a predictor over a finite time horizon can avoid this issue.

While a model-based control strategy is appealing, as this allows to incorporate additional information on the environment guiding the decision-making, it is also challenging with respect to the aforementioned difficulties. Hence, alternative model-free variants shall be briefly discussed here. Discrete formulations such as the proposed cluster-based control framework face the curse of dimensionality [35] where the high dimensionality of the problem as a result of the discretization prevents an exhaustive search for the optimal solution. Model-free extensions such as approximate dynamic programming exist to approximate the optimal cost function, e.g., using function approximators [36] or by successively improving the cost function through learning [22]. For instance, a recent study [37] employs Q-learning to determine the best control law for drag reduction on a cylinder. Alternatively, other optimization algorithms for the exploration of the solution space could be employed in order to circumvent this difficulty. For example, genetic algorithm, an evolutionary optimization method classically used for parameter optimization [38], aims to find the optimal solution by generating and evolving a set of candidate solutions based on the natural selection process. The clusters resulting from the state space discretization can also be interpreted as trust regions leading motivating trust-region reduced-order modeling [39,40].

The online capability of control strategies is critical for their application in realistic configurations. For a low number of sensors, e.g., of $\mathcal{O}(1)$–$\mathcal{O}(10^3)$, the involved calculations when applying the control law are sufficiently fast. If the flow state is based on velocity field measurements typically of $\mathcal{O}(10^5)$–$\mathcal{O}(10^7)$, the clustering algorithm is applied in the POD space as similarly done in this study. Then, the method will benefit from recent advances in compressed sensing [41] to find optimal sparse sensors in the high-dimensional velocity space that determine the instantaneous cluster affiliation.

Flow control has a long tradition in scientific and engineering applications. We believe that recent advances in data science [42,43] and machine learning techniques [37,44–46] will play an important role in flow control in the coming years. The cluster-based control framework, which is purely data-driven and determines optimal control laws in an unsupervised manner, contributes to this direction. The proposed approach offers a promising new path for controlling the ergodic measure on the attractor taking into account nonlinear actuation mechanisms.

Acknowledgements The authors acknowledge the funding and excellent working conditions of the project Separation Control—From passive to closed-loop design (SepaCoDe, ANR-11-BS09-018), the Chair of Excellence Closed-loop control of turbulent shear flows using reduced-order models (TUCOROM, ANR-10-CHEX-0015), both supported by the French Agence Nationale de la Recherche (ANR) and hosted by Institute PPRIME, the Collaborative Research Center (CRC 880) "Fundamentals of High Lift for Future Civil Aircraft" funded by the German Research Foundation (DFG) and hosted at the Technical University of Braunschweig, Germany, and the project "Novel Method of Physical Modal Basis Generation for Reduced Order Flow Models" funded by the Polish National Centre of Science under research grant no. 2011/01/B/ST8/07264. EK also thanks for the great support through the region Poitou-Charentes, the NSF PIRE Grant OISE-0968313, and the Air Force Research Lab under grant AFRL FA8651-16-1-0003. We appreciate valuable stimulating discussions with Bing Brunton, Steven Brunton, Eric Deem, Nicolai Kamenzky, Nathan Kutz and Robert Niven.

Appendix: Visualization of control laws

For the purpose of visualizing the similarity of the control laws, a distance matrix D

$$\mathsf{D}_{ij} = \sqrt{\frac{1}{2}\sum_{t=1}^{T}\left(b_i(\mathbf{s}_i(t)) - b_j(\mathbf{s}_i(t))\right)^2 + \frac{1}{2}\sum_{t=1}^{T}\left(b_i(\mathbf{s}_j(t)) - b_j(\mathbf{s}_j(t))\right)^2} \tag{34}$$

is defined. The $b_i(\mathbf{s}_i(t)) := \kappa^i(\mathbf{s}_i(t))$ is the time series of the control input based on sensor readings $\mathbf{s}_i$ when applying control law κ^i. The time series $b_i(\mathbf{s}_j(t)) := \kappa^i(\mathbf{s}_j(t))$ is obtained from evaluating κ^i using sensor readings $\mathbf{s}_j$ which are collected when κ^j was applied. This permutation is incorporated to ensure the symmetry of D. Note that $\mathbf{s} = \mathbf{a}$ in the case of full-state information.

A simple method that optimally preserves the control laws' pointwise distances is *multidimensional scaling* (MDS) [47,48]. For a given distance matrix according to a (possibly non-Euclidean) distance metric, MDS aims to find corresponding points in a low-dimensional subspace so that the distances between the points are preserved. We consider here in particular classical MDS (cMDS) which aims to approximate the distances in the subspace in a least mean square error sense. cMDS assumes that the distances are prescribed by the Euclidean metric which results in a connection between the Gram matrix $\mathsf{B} = \Gamma'\Gamma$, where $\Gamma = [\boldsymbol{\gamma}_1 \ldots \boldsymbol{\gamma}_N]$ contains the data points as columns, and the distance matrix D which can be computed by double-centering of B. Specifically, $\mathsf{B} = \mathsf{C}\mathsf{D}_2\mathsf{C}$ where $\mathsf{C} = \mathsf{I}_N - N^{-1}\mathsf{1}_N$ is the centering matrix with the $N \times N$ identity matrix I_N, a $N \times N$ matrix $\mathsf{1}_N$ of ones, and D_2 contains the squared distances between the $\boldsymbol{\gamma}_i$'s, i.e., $(\mathsf{D}_2)_{ij} := -\frac{1}{2}D_{ij}^2$. The points in Γ can then be recovered from the eigendecomposition $\mathsf{B} = \mathsf{V}\Lambda\mathsf{V}$ via $\Gamma = \Lambda^{1/2}\mathsf{V}^T$ where Λ contains the ordered eigenvalues λ_i, $i = 1, \ldots, N$, and V contains the eigenvectors as columns. Thus, a representation for the $\boldsymbol{\gamma}_i$'s can be determined from knowledge of the distance matrix. Keeping only the first r eigenvectors yields a r-dimensional approximation of the true γ_i's. If the distance matrix is computed using the Euclidean norm and N_z eigenvalues are exactly zero, there exists an exact representation of the points in a $N - N_z$-dimensional space. In particular, a two-dimensional subspace denoted by γ_1 and γ_2 for visualization purposes is of interest here. The solution can vary in terms of a translation, a rotation and reflections. Obviously, if the distance matrix is measured via the Euclidean metric, this method coincides with the POD, and the mean is at the origin and the axes are the POD eigenvectors [48]. If the distances are computed using a different metric such as (34), the method yields only an approximative representation.

References

1. Brunton, S.L., Noack, B.R: Closed-loop turbulence control: progress and challenges. Appl. Mech. Rev. **67**(5), 050801:01 (2015)
2. Lorenz, E.N.: Deterministic nonperiodic flow. J. Atmos. Sci. **20**, 130 (1963)
3. Lasota, A ., Mackey, M.C.: Chaos, Fractals, and Noise, 2nd edn. Springer, New York (1994)
4. Kaiser, E., Noack, B.R., Cordier, L., Spohn, A., Segond, M., Abel, M., Daviller, G., Östh, J., Krajnović, S., Niven, R.K.: Cluster-based reduced-order modeling of a mixing layer. J. Fluid Mech. **754**, 365 (2014)
5. Froyland, G.: Extracting dynamical behavior via Markov models. In: Mees, A.I. (ed.) Nonlinear Dynamics and Statistics, pp. 281–321. Birkhäuser, Boston (2001)
6. Hopf, E.: Statistical hydromechanics and functional analysis. J. Ration. Mech. Anal. **1**, 87 (1952)
7. Noack, B.R., Niven, R.K.: Maximum-entropy closure for a Galerkin system of incompressible shear flow. J. Fluid Mech. **700**, 187 (2012)
8. Munowitz, M., Pines, A., Mehring, M.: Multiple-quantum dynamics in NMR: a directed walk through Liouville space. J. Chem. Phys. **86**, 3172 (1987)
9. Brockett, R.W.: On the control of a flock by a leader. In: Proceedings of the Steklov Institute of Mathematics, vol. 268, pp. 49–57 (2010)
10. Brockett, R.W.: Minimizing attention in a motion control context. In: Proceedings of the 42nd IEEE Conference on Decision and Control, pp. 3349–3352 (2003)
11. Majumdar, A., Vasudevan, R., Tobenkin, M.M., Tedrake, R.: Convex optimization of nonlinear feedback controllers via occupation measures. Int. J. Robot. Res. **33**, 1209 (2014)
12. Brockett, R.: Notes on the control of the Liouville equation. In: Cannarsa, P., Coron, J .M. (eds.) Control of Partial Differential Equations. Cetraro, Italy 2010, pp. 101–129. Springer, Berlin Heidelberg (2012)
13. Bollt, E.M., Santitissadeekorn, N.: Applied and Computational Measurable Dynamics. Society for Industrial and Applied Mathematics, Philadelphia (2013)
14. Iversion, K.E.: A Programming Language, 2nd edn. Wiley, New York, NY, USA (1962)
15. Ulam, S.: A collection of Mathematical Problems. Interscience Publishers, New York (1960)
16. Li, T.Y.: Finite approximation for the Frobenius-Perron operator: a solution to Ulam's conjecture. J. Approx. Theory **17**(2), 177 (1976)
17. Bishop, C.M.: Pattern Recognition and Machine Learning. Springer, New York (2007)
18. Lloyd, S.: Least squares quantization in PCM. IEEE Trans. Inf. Theory **28**, 129 (1956). (Originally as an unpublished Bell laboratories Technical Note (1957))

19. Meyer, C.D.: Matrix Analysis and Applied Linear Algebra. Society for Industrial and Applied Mathematics, Philadelphia (2000)
20. Bang-Jensen, J., Gutin, G., Yeo, A.: When the greedy algorithm fails. Discrete Optim. **1**, 121 (2004)
21. Powell, Warren P.: Approximate Dynamic Programming: Solving the Curses of Dimensionality. Wiley, Hoboken, New Jersey (2007)
22. Sutton, R.S., Barto, A.G.: Reinforcement Learning: an Introduction. MIT Press, Cambridge (1998)
23. Sommer, F.: Mehrfachlösungen bei laminaren Strömungen mit druckinduzierter Ablösung: eine Kuspen-Katastrophe (trans.: Multiple solutions of laminar flows with pressure induced separation: a cusp catastrophe). Technical Report 7:206, Fortschrittberichte VDI, VDI Verlag, Düsseldorf (1992)
24. Hood, P., Taylor, C.: Finite element methods in flow problems. In: Oden, J.T., Gallagher, R.H., Zienkiewicz, O.C., Taylor, C. (eds) Navier-Stokes equations using mixed interpolation, pp. 121–132. Huntsville Press, University of Alabama (1974) (1974)
25. Morzyński, M.: Numerical solution of Navier-Stokes equations by the finite element method. In: Proceedings of SYMKOM 87, Compressor and Turbine Stage Flow Path—Theory and Experiment, pp. 119–128. (1987)
26. Afanasiev, K.: Stabilitätsanalyse, niedrigdimensionale modellierung und optimale kontrolle der kreiszylinderumströmung (trans.: Stability analysis, low-dimensional modeling, and optimal control of the flow around a circular cylinder). Ph.D. thesis, Fakultät Maschinenwesen, Technische Universität Dresden (2003)
27. Bao, F., Dallmann, U.C.: Some physical aspects of separation bubble on a rounded backward-facing step. Aerosp. Sci. Technol. **8**, 83 (2004)
28. Ho, C.M., Huerre, P.: Perturbed free shear layers. Ann. Rev. Fluid Mech. **16**, 365 (1984)
29. Holmes, P., Lumley, J.L., Berkooz, G., Rowley, C.W.: Turbulence, Coherent Structures, Dynamical Systems and Symmetry, 2nd edn. Cambridge University Press, Cambridge (2012)
30. Du, Qiang, Gunzburger, Max D.: Centroidal Voronoi Tessellation Based Proper Orthogonal Decomposition Analysis. Birkhäuser Basel, Basel (2003)
31. Schneider, T.M., Eckhardt, B., Vollmer, J.: Statistical analysis of coherent structures in transitional pipe flow. Phys. Rev. E **75**, 066313 (2007)
32. Giannakis, D., Majda, A.J.: Quantifying the predictive skill in long-range forecasting. Part I: Coarse-grained predictions in a simple ocean model. J. Climate **25** (6), 1793–1813 1793 (2012)
33. Brunton, S.L., Brunton, B.W., Proctor, J.L., Kaiser, E., Kutz, J.N.: Chaos as an Intermittently Forced Linear System. arXiv:1608.05306v1 (2016)
34. Froyland, G.: Statistically optimal almost-invariant sets. Physica D **200**(3), 205 (2005)
35. Bellman, R.E.: Adaptive Control Processes. Princeton University Press, New York (1961)
36. Bertsekas, D.P.: Dynamic Programming and Optimal Control, vol. II, 4th edn. Athena Scientific, Boston, MA (2012)
37. Guéniat, F., Mathelin, L., Hussaini, M.Y.: A statistical learning strategy for closed-loop control of fluid flows. Theor. Comput. Fluid Dyn. **30**, 497 (2016)
38. Wahde, M.: Biologically Inspired Optimization Methods: An Introduction. WIT Press, Southampton, UK (2008)
39. Amsallem, D., Cortial, J., Farhat, C.: In: 7th AIAA Aerospace Sciences Meeting Including The New Horizons Forum and Aerospace Exposition AIAA 2009-800, Orlando, Florida, 5–8 Jan 2009 (2009)
40. Amsallem, David, Zahr, Matthew J., Farhat, Charbel: Nonlinear model order reduction based on local reduced-order bases. Int. J. Numer. Methods Eng. **92**(10), 891 (2012). doi:10.1002/nme.4371
41. Brunton, B.W., Brunton, J.L., Proctor, S.L., Kutz, J.N.: Sparse sensor placement optimization for classification. SIAM. J. Appl. Math. **76**, 2099–2122 (2016)
42. Brunton, S.L., Proctor, J.L., Tu, J.H., Kutz, J.N.: Compressive sampling and dynamic mode decomposition. J. Comp. Dyn. **2**(2), 165–191 (2016)
43. Brunton, S.L., Proctor, J.L., Kutz, J.N.: Discovering governing equations from data: sparse identification of nonlinear dynamical systems. arXiv:1509.03580 (2015)
44. Tedrake, R., Jackowski, Z., Cory, R., Roberts, J. W., Hoburg, W.: Learning to fly like a bird. In: 14th International Symposium of Robotics Research (ISRR 2009), Lucerne, Aug 31–Sept 3, 2009 (2016)
45. Duriez, T., Parezanovic, V., Laurentie, J.C., Fourment, C., Delville, J., Bonnet, J.P., Cordier, L., Noack, B.R., Segond, M., Abel, M.W., Gautier, N., Aider, J.L., Raibaudo, C., Cuvier, C., Stanislas, M., Brunton, S.L.: Closed-loop control of experimental shear layers using machine learning (Invited). In: 7th AIAA Flow Control Conference AIAA Paper, Atlanta, Georgi (2014)
46. Parezanović, V., Cordier, L., Spohn, A., Duriez, T., Noack, B.R., Bonnet, J.P., Segond, M., Abel, M., Brunton, S.L.: Frequency selection by feedback control in a turbulent shear flow. J. Fluid Mech. **797**, 247 (2016)
47. Mardia, K.V., Kent, J.T., Bibby, J.M.: Multivariate Analysis. Academic Press, Cambridge (1979)
48. Cox, T.F., Cox, M.A.A.: Multidimensional Scaling, Monographs on Statistics and Applied Probability, vol. 88, 2nd edn. Chapman and Hall, London (2000)